CERN - EUROPEAN ORGANIZATION FOR NUCLEAR RESEARCH

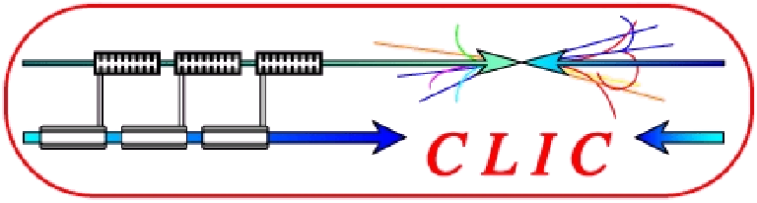

CLIC Note 732

EUROTeV-Report-2008-009

Conceptual design of a vacuum window at the exit of the CLIC post-collision line

A. Ferrari, V. Ziemann
Uppsala University, Sweden

In this paper, we present a design of the window between the accelerator vacuum and the beam dump at the end of the CLIC post-collision line. We propose to use a thick (1.5 cm) layer of carbon-carbon composite, with a thin (0.2 mm) leak-tight foil. The energy deposition and the temperature increase due to the beam impact, as well as the stress levels in the window, are estimated and we show that Aluminium is the most suitable material for the thin foil. At the beam impact, the temperature increase after the passage of a CLIC bunch train is of the order of 1 K and the subsequent (cyclic) thermal stress remains smaller than 1 MPa. As for the (static) mechanical stress, it is about 4 MPa in the beam impact region, and it goes up to 15 MPa near the lateral edges of the window. Still, these constraints are more relaxed than for the LHC dump window.

Geneva, Switzerland
February 15, 2008

1 Introduction

The Compact Linear Collider (CLIC) aims at multi-TeV e^+e^- collisions using the two-beam acceleration technology [1]. In the design used for this study [2], the accelerating gradient and the RF frequency are 150 MV/m and 30 GHz, respectively. In a high-energy e^+e^- linear collider such as CLIC, the incoming beams must be focused to very small spot sizes in order to achieve high charge densities and thereby reach the desired luminosity. As a result, the colliding beams experience strong electromagnetic fields at the interaction point. The subsequent bending of their trajectories leads to the emission of beamstrahlung photons, which can then turn into e^+e^- coherent pairs. A careful design of the post-collision lines must therefore be performed to transport all outgoing beams from the interaction point to the dump, with as small losses as possible.

A conceptual design of the CLIC post-collision line was presented in [3]. In a first step, it separates the various components of the outgoing beam in four extraction magnets, which provide a total bending angle of 3.2 mrad at 1.5 TeV. Following their physical separation from the other beam components, the particles of the coherent pairs with the wrong-sign charge are immediatly brought to their dump. The energy spectrum of the coherent pairs is derived from the vertical distribution of the wrong-sign charged beam. As for the disrupted beam and the beamstrahlung photons, they are transported in the same vacuum pipe to a common dump. The bend provided by the extraction magnets is followed by a bend in the opposite direction, in order to eventually have $D'_y = 0$. All beamstrahlung photons and charged particles with more than 15% of the nominal beam energy pass through the vertical chicane and reach the dump (the lost particles are absorbed in collimators). At the exit of the chicane, the low-energy particles of the disrupted beam, which still have $y' < 0$, receive a positive kick when passing through 16 vertically focusing quadrupoles (meanwhile, the high-energy core of the beam remains unaffected). This allows some flexibility in the design of the last section of the post-collision line, because the vertical rms size of the disrupted beam after the refocusing region decreases with the distance from the interaction point to the dump. An accurate analysis of the final transverse beam profiles allows to derive relevant information on the e^+e^- collisions. In particular, small vertical offsets in position and/or angle between the incoming beams, which affect the disruption process, can be identified by measuring the displacement and/or the distorsion of the outgoing beams. Note that these offsets may lead to additional losses along the post-collision line, however these only occur in the collimators.

In this paper, we focus on the design of the thin window that separates the beam dump from the accelerator vacuum, at the end of the CLIC post-collision line. This window must withstand a 20 MW beam power, not only when e^+e^- collisions occur (in which case the charged beams are widened at the interaction point), but also in the case of non-colliding beams. Due to their very low emittances, these undisrupted beams may be much smaller on the window, leading to a much higher local energy deposition.

In Section 2, we review the main parameters of the incoming beams at CLIC, as well as the transverse distributions of the non-colliding beams at the dump window. In Section 3, we discuss the various constraints to be considered when choosing a material for the window. We then estimate the energy deposition and the stress levels by means of numerical simulations in Section 4. Finally, a summary is given in Section 5.

2 Main characteristics of the non-colliding beams at the interaction point and at the dump window

The incoming beam parameters of the CLIC machine that we consider in this study are given in Table 1. A new set of beam parameters is under consideration for CLIC. However, we do not expect the transverse sizes of the undisrupted beam (and thereby our results) to be significantly affected.

Parameter	Symbol	Value	Unit
Centre-of-mass energy	E	3	TeV
Particles per bunch	N_b	2.56	10^9
Bunches per RF pulse	n	220	
Bunch spacing	Δt_b	0.267	ns
Repetition frequency	f	150	Hz
Primary beam power	P_b	20.4	MW
Horizontal normalized emittance	$(\beta\gamma)\epsilon_x$	660	nm.rad
Vertical normalized emittance	$(\beta\gamma)\epsilon_y$	10	nm.rad
Horizontal rms beam size	σ_x^*	60	nm
Vertical rms beam size	σ_y^*	0.7	nm
Rms bunch length	σ_z	30.8	μm
Full-width energy spread	σ_E/E	1	%
Peak luminosity	L	6.5	10^{34} cm^{-2} s^{-1}

Table 1: Beam parameters at the interaction point of the nominal CLIC machine [2].

At a distance s downstream of the interaction point, if there are no magnetic elements on the path of the undisrupted beam, the betatron functions are given by:

$$\beta(s) = \beta(IP) \times \left[1 + \left(\frac{s}{\beta(IP)}\right)^2\right], \tag{1}$$

where $\beta_x(IP) = 7$ mm and $\beta_y(IP) = 0.09$ mm. Note that the rms beam sizes derived from the β-functions and the emittances are somewhat smaller than those quoted in Table 1. The difference comes from the non-linearity of the Final Focus System, which yields larger effective spot sizes at the interaction point.

Figure 1 shows how the rms transverse sizes of the non-colliding beam depend on the distance to the interaction point, when all magnetic elements along the beam path are switched-off. For the conceptual design of the CLIC post-collision line performed in [3], the dump window was placed about 250 m downstream of the interaction point.

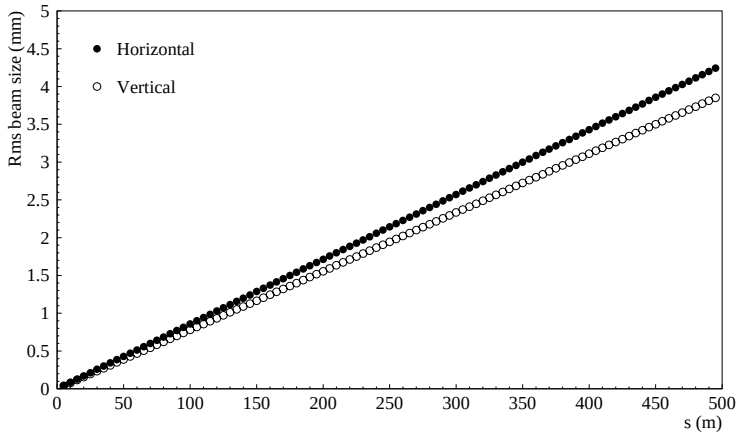

Figure 1: Transverse sizes of the undisrupted beam as a function of the distance s to the interaction point, when all magnetic elements are switched-off along the CLIC post-collision line.

Let us now consider a more realistic post-collision line, in which all dipole magnets and quadrupoles are switched-on. In that case, one must use simulation programs in order to estimate the transverse sizes of the undisrupted beam along the post-collision and at the dump window. In this study, we use the DIMAD particle tracking code [4].

Figure 2 shows the transverse distributions of the undisrupted beam obtained at the dump window, when it is located 247 m downstream of the interaction point and when all magnetic elements are switched-on along the post-collision line. The horizontal rms beam spot size is 2.2 mm. In the vertical direction, one obtains 3.3 mm. If there was no magnetic element along the beam path, the rms beam spot sizes would be 2.1 mm and 1.9 mm, respectively. The increase of the horizontal beam size is quite small and results from the transport through the quadrupoles, which are horizontally defocusing. In the vertical direction, the non-colliding beam is focused by the quadrupoles. On the other hand, the passage of the beam (with a non-zero energy spread) through the magnetic chicane leads to an enhancement of its vertical spot size, as a result of the dispersion ($D_y = 10.4$ cm).

Figure 3 shows how the rms transverse sizes of the non-colliding beam depend on the distance to the interaction point, when all magnetic elements along the beam path are switched-on.

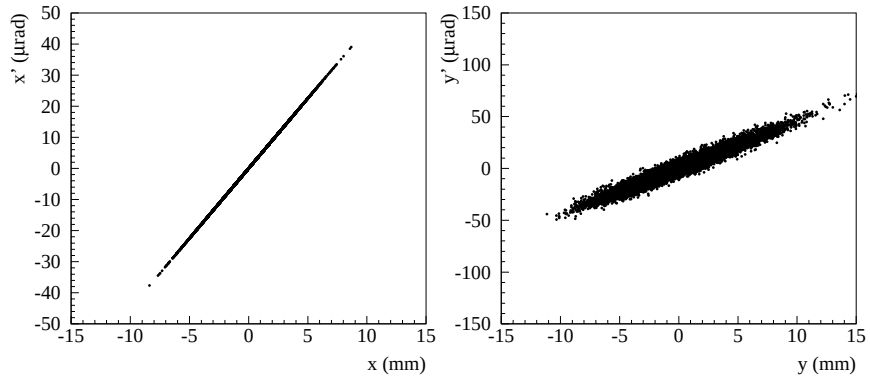

Figure 2: Transverse distributions of the undisrupted beam in the horizontal (left) and vertical (right) phase space, as obtained at the end of the CLIC post-collision line when all magnetic elements are switched-on.

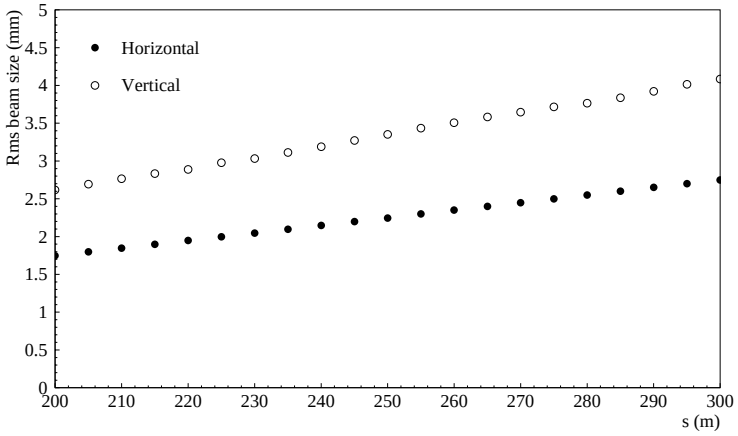

Figure 3: Transverse sizes of the undisrupted beam as a function of the distance s to the interaction point, when all magnetic elements are switched-on along the CLIC post-collision line.

3 Constraints on the window and material selection

The main purposes of the CLIC post-collision line are to transport as many particles as possible to the dump, as well as to obtain the most accurate image of the charged beams and the beamstrahlung photons after the e^+e^- collision. One must therefore keep the power losses at a low level. This is generally achieved by ensuring that the cross section of the pipe is large enough to accept most of the outgoing beams. In addition, one must take into account the dimension of the dump window and the beam spot size there, which both affect the level of stress in the window, and therefore its ability to withstand a 20 MW beam power.

When designing the dump window, one must make sure that its thickness d remains significantly smaller than one radiation length, which depends mostly on the atomic (or molecular) number Z and weight A of the material:

$$X_0 \simeq 716 \text{ g.cm}^{-2} \frac{A}{Z(Z+1)\ln(287/\sqrt{Z})}. \tag{2}$$

One should choose materials with a small value of Z, or use a very thin layer. However, in this latter case, the window may not be able to withstand the pressure difference ΔP between its two faces. Indeed, the corresponding static stress significantly depends on the size and thickness of the window. In particular, it increases with the size of the window and decreases with its thickness. Therefore, the use of a thick window with a low-Z material is preferable.

If $d \ll X_0$, then mostly ionization losses occur in the window. In the high-energy limit, the stopping power, expressed in $\text{MeV/g}\,\text{cm}^{-2}$, is [5]:

$$\left(\frac{dE}{\rho dx}\right) = 0.153536 \frac{Z}{A} B(T). \tag{3}$$

The stopping number $B(T)$ is given by:

$$B(T) = B_0(T) - 2\ln\left(\frac{E_p}{m_e c^2}\right) - 2\ln\left(\frac{p}{m_e c}\right) + 1. \tag{4}$$

Here, p and T are respectively the momentum and the kinetic energy of the incoming electron or positron. As for the plasma energy E_p, when expressed in eV, it is:

$$E_p = 28.816 \sqrt{\rho\, Z/A}. \tag{5}$$

Using $\tau = T/m_e c^2$, the function $B_0(T)$ is given by:

- for electrons,

$$B_0(T) = \ln(\tau^2(\tau+2)/2) + \frac{1 + \tau^2/8 - (2\tau+1)\ln 2}{(\tau+1)^2}, \tag{6}$$

- for positrons,

$$B_0(T) = \ln(\tau^2(\tau+2)/2) + 2\ln 2 - \frac{1}{12}\left(23 + \frac{14}{\tau+2} + \frac{10}{(\tau+2)^2} + \frac{4}{(\tau+2)^3}\right). \tag{7}$$

Note that the stopping power is the energy lost by the passing beam, and not the energy that is actually deposited in the target. A fraction of the lost energy may indeed escape from the dump window. The formulas of [5] thus give a conservative estimation of the energy deposited in the window.

The passage of a single bunch train with $n\,N_b$ particles through the dump window leads to an instantaneous temperature rise at the centre of the beam distribution. For the sake of simplicity, we assume a round Gaussian beam with a rms width $\sigma_{beam} = \sqrt{\sigma_x \cdot \sigma_y}$. If one neglects the temperature dependence of the heat capacity C and if one uses the stopping power instead of the actual deposited energy, the upper limit on the instantaneous local heating is [6]:

$$\Delta T_{inst} = \left(\frac{dE}{\rho dx}\right) \times \frac{n\,N_b}{2\pi C \sigma_{beam}^2}. \tag{8}$$

The largest temperature increase is caused by the non-colliding charged beam at 1.5 TeV (with a failure of every magnet along its path), for which σ_{beam} is the smallest (about 2 mm if the post-collision line is 250 m long).

For the sake of simplicity, we now consider a circular symmetry, which allows to simplify the analytical calculations. The passage of a bunch train through the window and its subsequent local heating occur at a repetition frequency of 150 Hz. The heat diffuses from the centre to the edge of the window, which is kept at a constant temperature T_{edge}. In cylindrical coordinates, the equilibrium temperature distribution is derived from the heat equation with no time dependence:

$$-\frac{k}{r}\frac{\partial}{\partial r} r \frac{\partial T}{\partial r} = p(r). \tag{9}$$

In this equation, k is the thermal conductivity (expressed in W/Km) and $p(r)$ is the power distribution (per unit volume). In the following, we proceed as in [6] and we assume that the power distribution is:

$$p(r) = n\,N_b\,f \times \left(\frac{dE}{dx}\right) \times \frac{2\sigma_{beam}^2}{\pi(r^2 + 2\sigma_{beam}^2)^2}. \tag{10}$$

It is similar to a Gaussian distribution, and it has the advantage that equation (9) can be solved analytically. The highest temperature (at the centre of the window) is:

$$T_0 = T_{edge} + \left(\frac{dE}{dx}\right) \times \frac{n\,N_b\,f}{4\pi k} \ln\left(1 + \frac{R^2}{2\sigma_{beam}^2}\right). \tag{11}$$

Materials with a small thermal conductivity k should be avoided as they may lead to a large equilibrium temperature T_0. In the worst case, the window may melt if the heat that is produced by the beam impact takes too much time to propagate towards the cooled edge, and thereby accumulates at the centre of the window.

Note that the only cooling process that we consider is the diffusion of heat from the beam spot at the centre of the window to its edge. At high temperatures, cooling may also occur through radiation (which varies like T^4). In addition, one may cool the dump window with a gas flow on its surface. For the sake of simplicity, these two additional cooling processes are not considered in the following.

To summarize, the window at the end of the CLIC post-collision line must have the following properties:

- its thickness must be significantly smaller than one radiation length so that only ionization losses occur in the window (low-Z materials should be used),
- it must withstand a pressure difference of about 1 atm,
- the heat produced by the beam impact must be transported away as quickly as possible, so materials with a small thermal conductivity k should be avoided.

At the Large Hadron Collider (LHC), a large diameter carbon-carbon composite dump window was designed [7] and the SIGRABOND 1501G grade material from SGL was selected. It has a mass per unit volume of 1.5 g.cm^{-3}, and its radiation length is 29 cm. This allows a relatively thick window, thereby reducing the mechanical stress due to the pressure difference. In addition, such a material has both a low elastic modulus E and a low thermal expansion coefficient α, which yields small thermal stresses. On the other hand, SIGRABOND 1501G is quite porous, so a thin leak-tight layer is needed to hold vacuum. It can be installed on the high pressure side of the window, since the outgasing rate of the carbon-carbon composite is low. If the thin foil is fully supported by the thick window, then the main load comes from the thermal stress, and one should choose a material with low elastic modulus and thermal expansion coefficient. For the LHC window, a 200 μm steel foil is used. At CLIC, one may choose other materials, with lower values of E and α, because the instantaneous temperature rise is far less dramatic than at LHC. For instance, Copper, Aluminium or Titanium can be envisaged for the thin leak-tight foil, whereas they were ruled out for the LHC dump window.

At this stage, one needs to perform numerical simulations for a more detailed design, e.g. to accurately determine the energy deposition in the thick carbon-carbon window and the thin leak-tight foil, the subsequent temperature increase and the corresponding cyclic thermal stresses. Also, since the CLIC carbon-carbon composite window does not actually have a circular shape, the mechanical stress can not be estimated with analytical formulas.

4 Numerical simulations of the energy deposition and the stresses in the CLIC dump window

4.1 Energy deposition in the CLIC dump window

In order to estimate the energy deposited by the CLIC electron or positron undisrupted beam in the dump window, the FLUKA program [8, 9] is used. We consider a target consisting of a 1.5 cm thick carbon-carbon composite window followed by a 0.2 mm thin foil, for which different materials (steel, Al, Ti, Cu) were tested. The properties of the various materials used in our FLUKA simulations are summarized in Table 2.

Material	Z	A	ρ (g/cm^3)
C-C composite	6	12.01	1.50
Steel 316	-	-	7.80
Aluminium	13	26.98	2.70
Titanium	22	47.87	4.54
Copper	29	63.55	8.96

Table 2: Properties of the materials considered for the CLIC dump window, including the thin leak-tight foil.

In order to compute the energy deposition as a function of the amount of material seen by the incident particles, the target is divided into several 0.1 mm thick layers along the beam axis in FLUKA. A similar meshing is also performed in the transverse plane.

Figure 4 shows the energy that is deposited by the 1.5 TeV undisrupted electron beam in each longitudinal layer of the CLIC dump window. In that case, a 0.2 mm thin steel foil was considered. Along the carbon-carbon composite window, one clearly observes an increase of the energy deposition with the amount of material seen by the incident beam, because some particle multiplication occurs (although a full electromagnetic shower has not developed yet). In the thin steel foil, the deposited energy is 1.63 MeV/g cm^{-2}. Actually, it does not significantly depends on the material that one chooses for the foil, since mostly ionization losses occur. Indeed, if one uses Al, Cu or Ti instead of steel, then the deposited energy becomes 1.72, 1.62 or 1.58 MeV/g cm^{-2}, respectively.

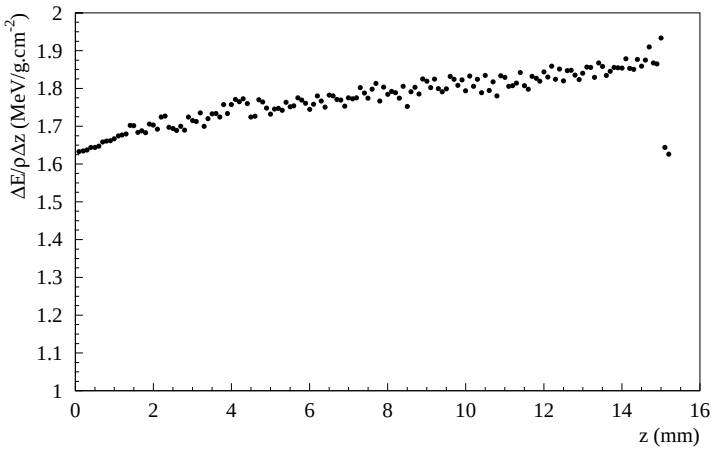

Figure 4: Energy deposited by the 1.5 TeV undisrupted electron beam (in MeV/g cm^{-2}) along the CLIC dump window: the last two points on the right-hand side of the plot correspond to the thin steel foil.

Figure 5 shows the transverse profiles of the energy deposition in the first and last layer of the dump window. In the first layer, the rms values of the horizontal and vertical energy deposition profiles are respectively $\sigma_x = 2.1$ mm and $\sigma_y = 1.9$ mm, which correspond to the transverse rms beam sizes. In the last layer of the dump window, σ_x and σ_y become respectively 2.2 mm and 2.0 mm. Therefore, no significant growth of the energy deposition profiles is observed, because no electromagnetic shower has developed.

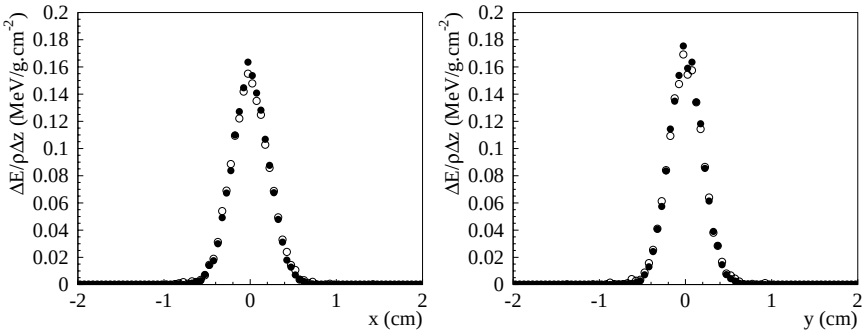

Figure 5: Horizontal and vertical profile of the energy deposition in the first (full circles) and last layer (open circles) of the dump window with a thin steel foil.

Having computed the energy deposition in small cells inside the dump window, one can then derive the local temperature increase. Here, the local heating due to the passage of one bunch train through the window is small, so one can neglect the variation of the heat capacity with the temperature. Using the deposited energy per unit length $\Delta E/\rho\Delta z$ and knowing its transverse distribution, one has:

$$\Delta T_{inst} = \left(\frac{\Delta E}{\rho \Delta z}\right) \times \frac{n\, N_b}{2\pi C \sigma_x \sigma_y}. \tag{12}$$

For the carbon-carbon composite, $C_{cc} = 0.53$ J/g K, so $\Delta T_{inst} = 1.1$ K at the entrance of the window and it does not vary by more than 10-15% along the beam path through the carbon-carbon composite window. For the thin foil with stainless steel, $\Delta T_{inst} = 1.0$ K. If we consider respectively Al, Ti or Cu instead, then the local temperature increase becomes 0.6 K, 1.0 K or 1.3 K. A summary of our results is given in Table 3.

If α is the thermal expansion coefficient and E is the elastic modulus of the chosen material, the (cyclic) thermal stress due to the (repetitive) temperature increase is:

$$\sigma_c = \alpha E \Delta T_{inst}. \tag{13}$$

This quantity was calculated for the carbon-carbon thick window, as well as for the thin leak-tight foil, using steel, Al, Ti or Cu. A summary of our results is given in Table 4.

Material	ρ (g/cm^3)	C (J/g K)	k (W/K cm)	ΔT_{inst} (K)
C-C composite	1.50	0.53	0.24	1.1
Steel 316	7.80	0.50	0.16	1.0
Aluminium	2.70	0.90	2.37	0.6
Titanium	4.54	0.53	0.22	1.0
Copper	8.96	0.38	3.90	1.3

Table 3: Properties of the various materials considered for the CLIC dump window, and instantaneous temperature increase due to the passage of one bunch train.

Material	E (GPa)	α (10^{-6} K^{-1})	σ_c (MPa)
C-C composite	70-85	7	0.6
Steel 316	200	11	2.2
Aluminium	70	23	1.0
Titanium	120	12	1.4
Copper	130	17	2.9

Table 4: Mechanical and thermal properties of the various materials considered for the CLIC dump window, and (cyclic) thermal stress due to the temperature increase at the beam impact.

In addition to the thermal stress, one must also consider the ability to transport away heat when choosing a material for the thin leak-tight foil. For the sake of simplicity, we assume a circular symmetry for the CLIC dump window, with a beam impact at its centre (with a repetition frequency of 150 Hz). The equilibrium temperature difference between the cooled edge and the centre of the window can be derived from equation (11). As a cross-check, one can also solve the (time-dependent) heat equation numerically.

In the following, we use:

$$p(r,t) = n\,N_b \times \left(\frac{dE}{dx}\right) \times \frac{2\sigma_{beam}^2}{\pi(r^2+2\sigma_{beam}^2)^2} \times \sum_n \delta(t-n/f). \tag{14}$$

The heat equation in the dump window can therefore be written as follows:

$$\frac{\partial T}{\partial t} = \frac{k}{\rho C}\left[\frac{1}{r}\frac{\partial}{\partial r} r \frac{\partial T}{\partial r}\right] + \sum_n \frac{\Delta T_{inst}}{(1+r^2/2\sigma_{beam}^2)^2}\,\delta(t-n/f). \tag{15}$$

The evolution of the temperature at the centre of the dump window, as well as its radial distribution, can be determined by numerically solving this equation, using a simplified one-dimensional version of the Crank-Nicholson algorithm [10]. A Gaussian temperature excitation was tested as well, leading to very similar results.

We consider a round window with a cross section of 0.2 m^2 (i.e. a radius of 25 cm), placed about 250 m downstream of the interaction point. In the worst case scenario (with a failure of all magnets along the CLIC post-collision line), the transverse beam size σ_{beam} is 2 mm. Figure 6 shows the time evolution of the temperature difference between the beam spot and the cooled edge at the entrance of a round thick carbon-carbon window, over the first half second and over 2000 s.

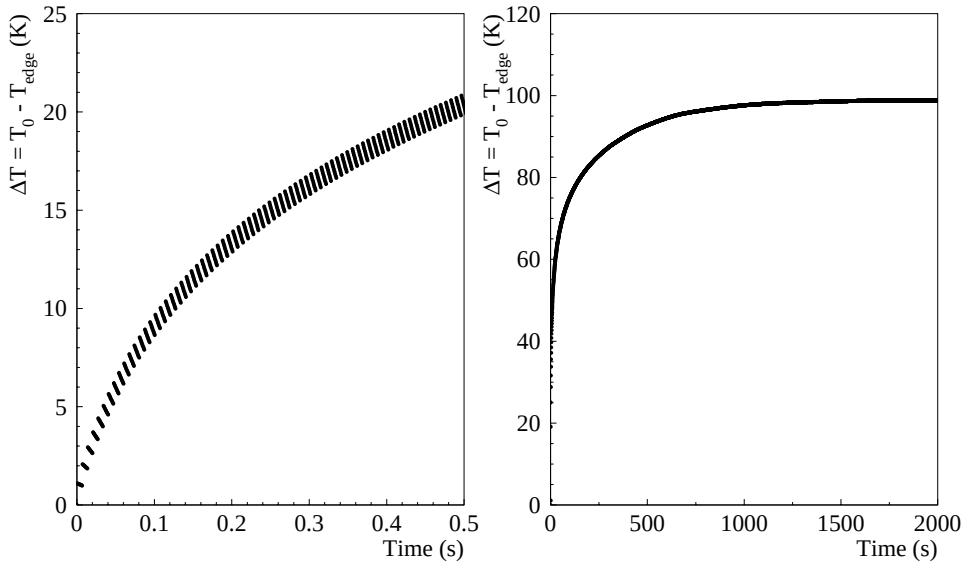

Figure 6: Time evolution of the temperature difference between the centre and the edge of a round window, just after the first beam impact (left), where the 150 Hz oscillations are clearly visible, and over 2000 s (right).

When solving the heat equation numerically, we find that the temperature difference between the centre and the edge of a round window is 98 K at the equilibrium, in very good agreement with the analytical prediction of equation (11), which is 99 K. This remains far below the melting temperature of the SIGRABOND 1501G carbon-carbon composite, ensuring a safe operation from a thermal point of view.

The same analysis was performed for the thin leak-tight foil. While the equilibrium temperature difference between the centre and the edge of a round window remains at a reasonable level for Al and Cu (respectively 19 K and 36 K), the results that were obtained for steel and Ti (about 700 K and 300 K, respectively) suggest that these two materials should be avoided, due to their small diffusion constant $k/\rho C$. Finally, since the thermal stress obtained for Aluminium is about three times smaller than for Copper (see Table 4), it seems to be the most suitable material for the thin leak-tight foil. The tensile strengths of Aluminium and Copper depend on the purity of the material or the alloy that one uses. In any case, they typically reach a few hundred MPa, i.e. well above the thermal stress in the thin foil.

4.2 Computation of the mechanical stress

In addition to the cyclic thermal stress, the dump window must withstand the pressure difference ΔP between its two faces. The corresponding static stress σ_s significantly depends on the shape of the window, which is not circular. This assumption was only made to easily solve the heat equation and compare the equilibrium temperatures for the various materials considered in this study. However, this simplification can not be used anymore when estimating the mechanical stress, because it does not have a local effect (as opposed to the temperature increase and the thermal stress, which are directly related to the beam impact). Therefore, one must use a finite element method with a simulation tool such as ANSYS [11] in order to better estimate the mechanical stress. In our simulation studies, the window has a racetrack shape, with a straight length of 50 cm and a radius of 13 cm for the two half-circles. The undisrupted beam hits the window at the centre of the upper circle, see Figure 7. For the computation of the mechanical stress, we perform ANSYS simulations of the carbon-carbon composite only, because the Aluminium thin leak-tight foil is fully supported by the thick window.

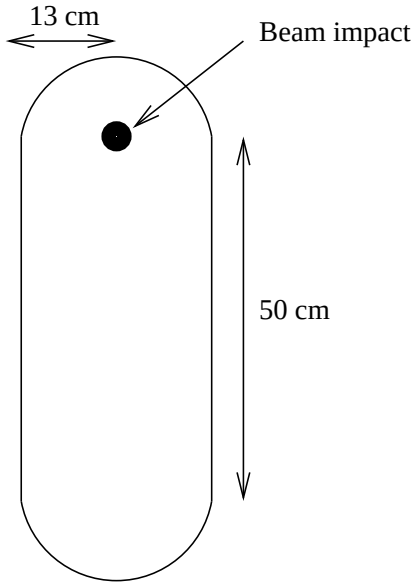

Figure 7: Schematic layout of the window used in ANSYS for the computation of the mechanical stress.

The carbon-carbon composite sheet is considered as a thin plate, supported around its circumference. In order to compute the deformation and the mechanical stress with ANSYS, one only needs the elastic modulus and the Poisson ratio, which is defined as the ratio between the transverse strain (normal to the applied load) and the axial strain (in the direction of the applied load). However, our results practically do not depend on the Poisson ratio, so the only relevant parameter is the elastic modulus, for which we use $E = 70$ GPa.

Assuming an atmospheric pressure load of 0.1 MPa (uniformly distributed over the cross section of the carbon-carbon composite sheet), as well as no degree of freedom around the window circumference, i.e. where it is fixed to its support, our simulations yield a maximal mechanical stress of 14.8 MPa, together with a displacement of 0.06 mm at the centre of the window. Figure 8 shows the distribution of the stress intensity over the window.

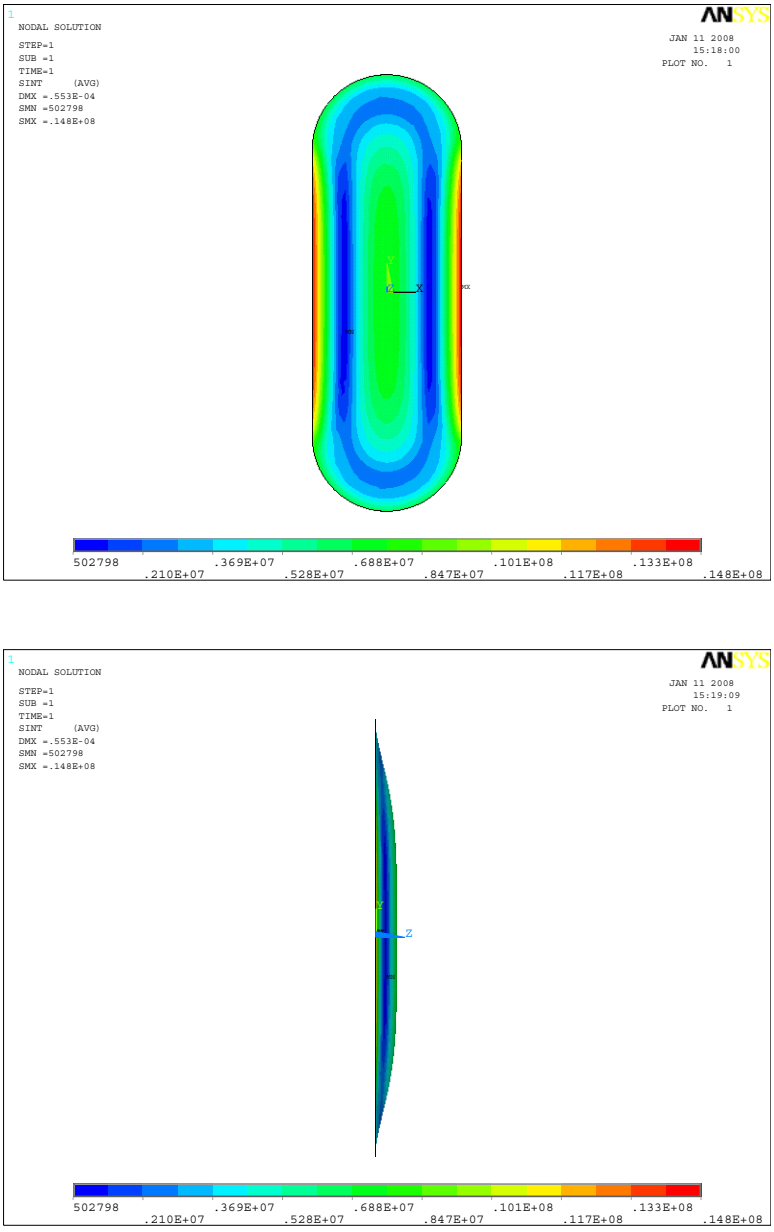

Figure 8: Mechanical stress intensity in the CLIC dump window.

The largest stress is obtained on the lateral edges of the window, where there is almost no thermal stress. In the beam impact region, σ_s is about three times smaller, about 4 MPa. The tensile strength of the SIGRABOND 1501G carbon-carbon composite is much larger (350 MPa typically) and, furthermore, it is not significantly affected by (thermal) load alternations.

For the LHC circular dump window, the pressure load was determined using analytical formulas for a thin plate under uniform pressure (0.14 MPa) with small deflections. The analysis reported in [7] yielded a maximal mechanical stress of 69 MPa as well as a deflection of 2.9 mm. As a cross-check, we performed ANSYS simulations of the carbon-carbon composite LHC round window and found similar results. As far as the static mechanical constraints are concerned, the CLIC dump window should operate in more relaxed conditions than its LHC counterpart (note that the dump window area is about twice smaller for CLIC than for LHC).

A way to reduce the pressure difference and thereby the mechanical stress is to use two windows. The thin region between them could be filled with a cooling gas, or with a laminar flowing sheet of water. If the water flows horizontally, monitoring its vertical temperature distribution, for instance with the interferometric thermometer proposed in [12], may provide a signal related to the vertical energy deposition and thereby information on the beam profile at the dump window and, in turn, on its angular divergence at the interaction point. In addition, the use of two windows is preferable for safety issues, since it is unlikely that both break simultaneously. One may then monitor the tightness of one window and rapidly switch-off CLIC in case of failure.

5 Conclusion

In this paper, we have performed analytical calculations and numerical simulations of the energy deposition, the temperature increase due to the beam impact and the stresses in the window between the accelerator vacuum and the beam dump at the end of the CLIC post-collision line. Similarly to the design considered for the LHC dump window, we use a thick (1.5 cm) layer of carbon-carbon composite (SIGRABOND 1501G) and a thin (0.2 mm) leak-tight foil made of Aluminium. This material both yields a small thermal stress and allows to quickly transport away the heat resulting from the beam impact. In our design, the thickness of the window remains significantly smaller than one radiation length (which ensures that only ionization losses occur during the beam passage) but still large enough to withstand the pressure difference.

At the beam impact, the temperature increase is of the order of 1 K and the subsequent thermal stress remains smaller than 1 MPa in both the carbon-carbon window and the Aluminium foil. As for the static mechanical stress, it is about 4 MPa in the beam impact region, but goes up to 15 MPa near the lateral edges of the window (where there is no thermal stress). Furthermore, the equilibrium temperatures at the beam impact

in both the carbon-carbon thick window and the leak-tight thin foil remain well below the melting temperature. Taking into account both the thermal and mechanical loads, we showed that the total stress is well below the tensile strength, i.e. the stress level at which failures start to occur.

The CLIC beam parameters were recently reviewed and updated. The performance of the window mostly depends on the spot size of the undisrupted beam (and thus the overall length of the post-collision line) as well as on the beam current (i.e. the number of particles per bunch train and the repetition frequency). We do not expect these quantities to change significantly, so our design should be valid with the new CLIC beam parameters as well. Still, we plan to review the design of both the post-collision line layout and the window at its end in a future study.

Acknowledgements

This work is supported by the Commission of the European Communities under the 6^{th} Framework Programme "Structuring the European Research Area", contract number RIDS-011899.

The authors wish to thank J. Vollaire and M. Lantz for their help with FLUKA, as well as B. Goddard, R. Veness and W. Weterings for fruitful discussions on the design of the dump window and the use of ANSYS.

References

[1] I. Wilson, "The compact linear collider CLIC", CLIC note 617, CERN-AB-2004-100, published in Phys. Rep. 403-404 (2004) 365-378.

[2] F. Tecker *et al.*, "Updated CLIC parameters 2005", CLIC note 627.

[3] A. Ferrari, "Conceptual design of a post-collision transport line for CLIC at 3 TeV", CLIC note 704, EUROTeV-Report-2007-001.

[4] http://www.slac.stanford.edu/accel/ilc/codes/dimad

[5] S.M. Seltzer and M.J. Berger,"Improved procedure for calculating the collision stopping power of elements and compounds for electrons and positrons", Int. J. Appl. Radiat. Isot. Vol. 35, No. 7 (1984) 665-676.

[6] M. Seidel, "An Exit Window for the TESLA Test Facility", DESY-TESLA 95-18.

[7] R. Veness, B. Goddard, S.J. Mathot, A. Presland and L. Massidda, "Design of the LHC beam dump entrance window", proceedings of EPAC06, Edinburgh, Scotland.

[8] A. Fasso, A. Ferrari, J. Ranft and P.R. Sala, "FLUKA: a multi-particle transport code", CERN-2005-010, INFN/TC_05/11, SLAC-R-773.

[9] A. Fasso, A. Ferrari, S. Roesler, P.R. Sala, G. Battistoni, F. Cerutti, E. Gadioli, M.V. Garzelli, F. Ballarini, A. Ottolenghi, A. Empl and J. Ranft, "The physics models of FLUKA: status and recent developments", Computing in High Energy and Nuclear Physics 2003 Conference (CHEP2003), La Jolla, CA, USA, March 24-28, 2003, paper MOMT005, eConf C0303241, hep-ph/0306627.

[10] E. J. Davison, "A high-order Crank-Nicholson technique for solving differential equations", Comput. J 10 (1967), 195-197.

[11] http://www.ansys.com/ (ANSYS v. 11.0 Academic Research).

[12] V. Ziemann, "Ideas for an Interferometric Thermometer", Nucl. Inst. and Meth. A564 (2006) 587-589.